nature chemistry

ARTICLES

https://doi.org/10.1038/s41557-019-0220-2

Ion-mediated hydrogen-bond rearrangement through tunnelling in the iodide–dihydrate complex

Pushp Bajaj[1], Jeremy O. Richardson[2] and Francesco Paesani[3]*

A microscopic picture of hydrogen-bond structure and dynamics in ion hydration shells remains elusive. Small ion–dihydrate molecular complexes are ideal systems with which to investigate the interplay and competition between ion–water and water–water interactions. Here, state-of-the-art quantum dynamics simulations provide evidence for tunnelling in hydrogen-bond rearrangements in the iodide–dihydrate complex and show that it can be controlled through isotopic substitutions. We find that the iodide ion weakens the neighbouring water–water hydrogen bond, leading to faster water reorientation than in the analogous water trimer. These faster dynamics, which are apparently at odds with the slowdown observed in the first hydration shell of iodide in solution, can be traced back to the presence of a free OH bond in the iodide–dihydrate complex, which effectively triggers the overall structural rearrangements within it. Besides providing indirect support for cooperative hydrogen-bond dynamics in iodide solutions, the analysis presented here suggests that iodide ions may accelerate hydrogen-bond rearrangements at aqueous interfaces, where neighbouring water molecules can be undercoordinated.

Determining the driving forces that govern ion hydration is key to the molecular-level understanding of a broad range of chemical transformations in aqueous environments. For example, ions play important roles in acid–base chemistry and catalytic processes[1,2], in the stabilization of biomolecules, as well as in mediating protein–protein interactions and intracellular signal transduction[3–5]. In the atmosphere, ionic clusters carry electric currents and are involved in the formation and evolution of aerosol particles[6,7]. In materials science, ionic solutions are central to many devices, including electrolytic cells, capacitors and batteries[8].

Because of long-range Coulomb interactions, ions do not exist as isolated species under equilibrium in the gas phase but form neutral ionic aggregates (for example, ionic salts). Completely different behaviour is observed when ions are dissolved in water. In this case, ion–ion interactions are mediated by the presence of water molecules that allow ions to exist as individual solvated species, up to saturation. Ion stabilization in aqueous solutions results from the interplay of ion–water interactions, which primarily depend on the nature of the ion, and entropic contributions, which are associated with solvent reorganization around the charged species. Although the water hydrogen -bond network is expected to adapt to the presence of ions, the extent to which its structural, thermodynamic and dynamical properties change remains an open question[9].

Halide ions represent a prototypical class of ionic systems, exhibiting large variations in size, charge density and polarizability. General correlations have been derived between the chemical nature of these ions and the properties of the surrounding hydrogen bond network in solution, with smaller fluoride ions, on the one hand, establishing stronger hydrogen bonds with water, while larger and more polarizable iodide ions, on the other hand, induce relatively larger structural rearrangements on the surrounding hydrogen -bond network, at least locally. Ultrafast vibrational spectroscopy experiments indicate that the dynamics of water in the first solvation shells of halide ions is significantly slowed down compared to that observed in pure water[10]. Ion-specific effects have been found at the air–water interface, suggesting that larger and more polarizable halide ions, such as iodide, may exhibit a relatively higher propensity for the interface than smaller halides and cations[6,11].

Given the recent advances in high-resolution vibrational spectroscopy as well as progress in the development of accurate quantum dynamics methods, small halide–water clusters represent ideal systems for characterizing the interplay between ion–water and water–water interactions, energetic and entropic contributions, and nuclear quantum effects in hydrogen-bond rearrangements around individual halide ions[12–18]. Measurements of vibrational predissociation spectra combined with successive isotopic substitutions have allowed for precisely probing possible hydrogen-bonding environments and monitoring their evolution as a function of temperature[19,20]. In particular, the vibrational spectra of the iodide–dihydrate complex, $I^-(H_2O)_2$ (refs. [19,20]), measured at low temperature in the water OH bond stretching region, exhibit a well-defined pattern consisting of four distinct peaks at 3,344 cm^{-1}, 3,516 cm^{-1}, 3,619 cm^{-1} and 3,684 cm^{-1}. These peaks can be assigned to specific hydrogen-bonding environments within the minimum energy structure of $I^-(H_2O)_2$, corresponding to a 'closed' configuration with an intact water–water hydrogen bond (Fig. 1). As the temperature increases above 50 K, a new, broad peak starts emerging at 3,440 cm^{-1} which is accompanied by the simultaneous disappearance of the initial pattern observed at low temperature, indicating that the complex undergoes significant temperature-dependent hydrogen-bond rearrangements.

In this study, we combine state-of-the-art quantum simulations with many-body representations of the underlying molecular interactions to provide a microscopic characterization of the temperature-dependent hydrogen-bond dynamics in $I^-(H_2O)_2$. Our analysis provides unambiguous evidence for hydrogen-bond rearrangements via tunnelling mediated by the presence of the iodide ion. Through selective isotopic substitutions, we further demonstrate that tunnelling is still observed, although to a lesser extent, in $I^-(D_2O)_2$, while it is suppressed in the asymmetric $I^-(HOD)(D_2O)$ isotopologue, in

[1]Department of Chemistry and Biochemistry, University of California, San Diego, La Jolla, CA, USA. [2]Laboratory of Physical Chemistry, ETH Zürich, Zürich, Switzerland. [3]Department of Chemistry and Biochemistry, Materials Science and Engineering, and San Diego Supercomputer Center, University of California, San Diego, La Jolla, CA, USA. *e-mail: fpaesani@ucsd.edu

a

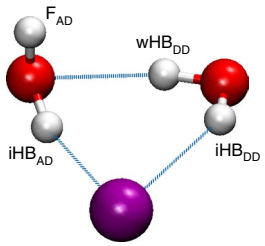

b

Mode	$I^-(H_2O)_2$		$I^-(D_2O)_2$	
	Theory	Experiment	Theory	Experiment
iHB_{AD}	3,337	3,344	2,475	2,480
iHB_{DD}	3,500	3,504/3,516	2,578	2,589
wHB_{DD}	3,594	3,619	2,663	2,684
F_{AD}	3,684	3,684	2,719	2,719

Fig. 1 | Ground-state geometry and OH-stretch vibrational frequencies of the iodide–dihydrate complex. a, Global minimum energy ('closed') configuration of the iodide–dihydrate complex. The iodide ion (I^-) is shown in purple, and the oxygen (O) and hydrogen (H) atoms of the water molecules are shown in red and white, respectively. The hydrogen atoms of the double-donor (DD) water molecule are labelled iHB_{DD} and wHB_{DD} to indicate the two hydrogen bonds to the iodide ion and single-acceptor/single-donor (AD) water molecule, respectively. The H atoms of the AD water molecule are labelled iHB_{AD} and F_{AD} to indicate the hydrogen bond to the iodide ion and the free OH bond, respectively. **b**, Theoretical and experimental[20] OH and OD stretching frequencies (in cm^{-1}) of $I^-(H_2O)_2$ and $I^-(D_2O)_2$ complexes in the corresponding global minimum energy configurations. The close agreement between the theoretical and experimental values demonstrates the high accuracy of the MB-nrg PEFs.

which the hydrogen atom remains locked-in in the free position at low temperature. As the water–water hydrogen bond starts breaking at temperatures above ~75 K, the complex transitions from the 'closed' to an 'open' configuration, corresponding to a dynamic configuration with two dangling water molecules hydrogen-bonded to the iodide ion but not to each other, which becomes the most stable structure of the complex above 150 K (Supplementary Section 2).

Results

Tunnelling pathways and ground-state hydrogen-bond rearrangements. As shown in Fig. 1, the minimum energy structure of the iodide–dihydrate complex, corresponding to the 'closed' configuration, is characterized by a double-donor (DD) water molecule that donates single hydrogen bonds to both the iodide ion and a second water molecule that acts as a single-acceptor/single-donor (AD), donating one hydrogen bond to the iodide ion and having one free OH bond. Because the four OH bonds in $I^-(H_2O)_2$ experience different hydrogen-bonding environments, they are associated with distinct stretching frequencies, spanning a range of ~400 cm^{-1} (Fig. 1b). For both $I^-(H_2O)_2$ and $I^-(D_2O)_2$, the anharmonic frequencies calculated by combining the local-mode[21,22] and local-monomer[23] methods with the iodide-water MB-nrg many-body potential energy function (PEF) of ref. [24] are always within 25 cm^{-1} of the corresponding experimental values, providing support for the accuracy of the theoretical approach employed in this study[25].

It has been established that tunnelling pathways leading to hydrogen-bond rearrangements, and tunnelling splittings of otherwise degenerate energy levels, exist in halide–water dimers[15,17,18] as well as in the water trimer, which, in its minimum energy configuration, exhibits a cyclic structure analogous to that of the iodide–dihydrate complex[26–29]. To determine possible ground-state (0 K) tunnelling pathways and associated tunnelling splittings, in $I^-(H_2O)_2$ and its isotopologue, $I^-(D_2O)_2$, ring-polymer instanton (RPI) calculations[29,30] were performed (see Supplementary Section 1 for specific details). Three feasible tunnelling pathways, namely, iodide–water hydrogen-bond bifurcation, water–water hydrogen-bond bifurcation and flip rotation are identified, as shown in Fig. 2b–d. Each of the first two pathways involves the breaking and forming of a single hydrogen bond, while the third pathway corresponds to the out-of-plane rotation of the free OH bond of the AD water molecule. The associated energy splitting patterns calculated by diagonalizing the corresponding tunnelling matrices[29] are shown in Fig. 2a. Within the RPI formalism, the dimensions of the tunnelling matrices represent the number of identical versions of each molecular complex, 16 in the case of the iodide–dihydrate complex, which are generated through permutations of the hydrogen (or deuterium) atoms and the inversion operation[29,30]. Each off-diagonal matrix element corresponds to the tunnelling associated with a distinct pathway connecting two different versions of the same complex[29]. The individual tunnelling matrix elements associated with the three tunnelling pathways are given in Table 1. The full 16 × 16 tunnelling matrix used in the calculations of the tunnelling splitting patterns and the resulting tunnelling timescales is provided in Supplementary Section 4. As expected, given the heavier mass of deuterium, the RPI calculations predict smaller tunnelling splittings for $I^-(D_2O)_2$ than $I^-(H_2O)_2$.

The RPI results provide unambiguous evidence for the existence of well-defined tunnelling pathways. However, current experimental vibrational spectra for ionic clusters are not able to resolve such fine detail. Instead, determining the associated timescales is critical to guiding comparisons between theory and experiment. The tunnelling dynamics within the different isotopologues of the iodide–dihydrate complex—$I^-(H_2O)_2$, $I^-(D_2O)_2$ and $I^-(HOD)(D_2O)$—can be determined by monitoring the time evolution of the corresponding hydrogen-bond arrangements through propagation of the time-dependent Schrödinger equation under the action of the tunnelling Hamiltonian (Supplementary Section 4). Here, we assume that at low enough temperature, only the lowest tunnelling-vibrational states will be occupied. Figure 3a,b shows, respectively, the probabilities for a hydrogen atom of $I^-(H_2O)_2$ and a deuterium atom of $I^-(D_2O)_2$, initially located in the free position ($t = 0$, blue trace), to be found in any of the four different positions, represented by the four different colours (see schematic in Fig. 3), at a later time t. Also shown in Fig. 3c are the corresponding probabilities for the hydrogen atom of HOD in $I^-(HOD)(D_2O)$. As expected from the tunnelling splitting values, $I^-(H_2O)_2$ displays faster tunnelling dynamics than $I^-(D_2O)_2$. On the other hand, in the ground state of $I^-(HOD)(D_2O)$, the hydrogen atom is predicted to remain effectively locked-in in the free position. Here, we assume that the coupling between wells is the average of the $I^-(H_2O)_2$ and $I^-(D_2O)_2$ clusters, but that the zero-point energy of each well is different. It is thus the asymmetry within the $I^-(HOD)(D_2O)$ complex that leads to destruction of the quantum coherence.

Direct insights into the effects of iodide on the water–water hydrogen-bond rearrangement are gained from the comparison reported in Table 1 between the tunnelling matrix elements calculated for both $I^-(H_2O)_2$ and $I^-(D_2O)_2$, and the corresponding values for the water dimer and trimer[29]. Although both water–water

Table 1 | Comparisons of tunnelling splittings in the iodide–dihydrate complex and analogous water complexes.

	$(H_2O)_2$	$(H_2O)_3$	$I^-(H_2O)_2$	$(D_2O)_2$	$(D_2O)_3$	$I^-(D_2O)$
Iodide–water bifurcation	–	–	5.9	–	–	1.2
Water–water bifurcation	0.035	~0.01	1.7	2.7×10^{-4}	3.0×10^{-5}	0.29
Flip rotation	5.5	50	0.09	0.6	18	3.4×10^{-3}

Shown are tunnelling matrix elements, $-h$ (in cm^{-1}), for the iodide–water and water–water hydrogen-bond bifurcations, and flip rotation pathways calculated for the water dimer and trimer (ref. [29]), and $I^-(H_2O)_2$ and $I^-(D_2O)_2$ isotopologues of the iodide–dihydrate complex (this work). It should be noted that the flip rotation in the water dimer follows a slightly different mechanism from that observed in the water trimer and iodide–dihydrate complex; however, this still does not involve the breaking of any hydrogen bonds as in the other two complexes.

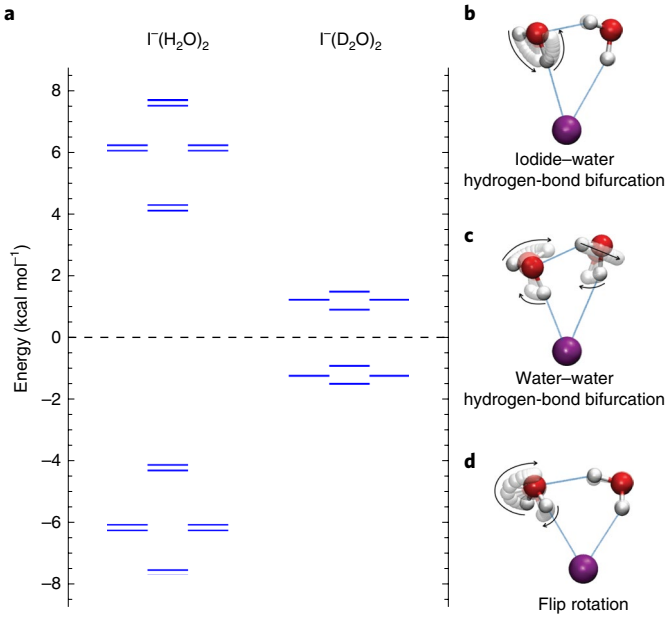

Fig. 2 | Ground-state tunnelling pathways and splitting pattern in the iodide–dihydrate complex. a–d, Ground-state tunnelling splitting patterns (**a**) in the $I^-(H_2O)_2$ (left) and $I^-(D_2O)_2$ (right) isotopologues of the iodide–dihydrate complex that result from the iodide–water hydrogen-bond bifurcation (**b**), water–water hydrogen-bond bifurcation (**c**) and flip rotation (**d**) tunnelling pathways shown in the schematics. The doublets in the splitting patterns of $I^-(D_2O)_2$ are not resolved on this energy scale. Larger splittings are observed in the $I^-(H_2O)_2$ isotopologue due to the H atoms being lighter and, consequently, exhibiting more pronounced quantum-mechanical behaviour than the corresponding D atoms.

hydrogen-bond bifurcation and flip rotation follow pathways similar to those found in pure water complexes, the tunnelling timescales (which, for degenerate rearrangements, are inversely proportional to the associated tunnelling splittings; Supplementary Section 4) are significantly different. In particular, the water–water hydrogen-bond bifurcation dynamics in the iodide–dihydrate complex is orders of magnitude faster than in the water trimer. The presence of the iodide ion drastically weakens the neighbouring water–water hydrogen bond, resulting in an energy barrier for the water–water hydrogen-bond bifurcation in the iodide–dihydrate complex of 0.52 kcal mol^{-1}, which is more than a factor of four lower than that in the water trimer (~2.34 kcal mol^{-1}). Importantly, the flip rotation in the pure water complexes is faster than all water–water hydrogen-bond bifurcations, because it does not require breaking any hydrogen bond. However, the same trend is not followed in the iodide–dihydrate complex, for which the flip rotation is particularly slow. This slower dynamics is explained by considering that the energy barrier for the flip rotation (1.11 kcal mol^{-1}) in the iodide–dihydrate complex is more than two times higher than the barrier associated with the iodide–water (0.47 kcal mol^{-1}) and water–water (0.52 kcal mol^{-1}) hydrogen-bond bifurcations, and more than four times higher than those associated with flip rotation in the water trimer (0.24 kcal mol^{-1})[29]. The high energy barrier in the iodide–dihydrate complex could be attributed to the large positive change in the electrostatics interactions in the planar transition state relative to the minimum energy configuration (Supplementary Section 4).

Because minimal rearrangement of the oxygen atoms is required for the iodide–water hydrogen-bond bifurcation, the associated pathway is characterized by a potential energy barrier that is lower by ~0.06 kcal mol^{-1} and narrower by ~24°, in full-width at half-maximum, than that found along the water–water hydrogen-bond bifurcation (Fig. 4). As a consequence, the iodide–water hydrogen-bond bifurcation is faster than the water–water hydrogen-bond bifurcation, resulting in a larger tunnelling splitting. The difference between the H–O–I angles (denoted as α), corresponding to the free OH bond, and the hydrogen-bonded-to-iodide OH bond within the same water molecule is used in Fig. 4 as a collective variable to describe the iodide–water hydrogen-bond bifurcation pathway. The difference between the H–O–I–O′ dihedrals (denoted as δ), corresponding to the free OH bond, and the hydrogen-bonded-to-water OH bond is used as a collective variable for the water–water hydrogen-bond bifurcation pathway. It should be noted that, although the shape of the two barriers would be different if only one angle (dihedral) were used instead of the difference between two angles (dihedrals), the relative differences between the two barriers would be independent of the specific choice of the collective variable.

Temperature dependence and hydrogen-bond dynamics. Previous studies determined that the water–water hydrogen bond in the iodide–dihydrate complex starts breaking at ~100 K, which leads to an open configuration with two dangling water molecules hydrogen-bonded to the iodide ion. To monitor the equilibrium between closed and open configurations and characterize the effects of tunnelling on the hydrogen-bond dynamics as a function of temperature, path-integral molecular dynamics (PIMD) simulations were carried out for $I^-(H_2O)_2$ and $I^-(D_2O)_2$ between 10 K and 200 K. In agreement with the analysis of vibrational predissociation spectra[19], PIMD simulations predict that both complexes exist predominantly in closed configurations below 100 K (Supplementary Section 2).

Additional insights into the role played by tunnelling in hydrogen-bond rearrangements within $I^-(H_2O)_2$ and $I^-(D_2O)_2$ at finite temperature can be gained from the analysis of one-dimensional (1D) quantum free energies along the two collective variables describing iodide–water and water–water hydrogen-bond bifurcations calculated from the PIMD trajectories, which are shown in Fig. 4. For comparison, also shown are the associated minimum energy paths (MEPs) on the underlying Born–Oppenheimer potential energy surface. Below 50 K, both quantum free energy barriers for the two hydrogen-bond bifurcations are significantly lower than the corresponding Born–Oppenheimer potential energy barriers. This implies that the OH and OD bonds in $I^-(H_2O)_2$ and $I^-(D_2O)_2$, respectively, undergo frequent interconversions between the four

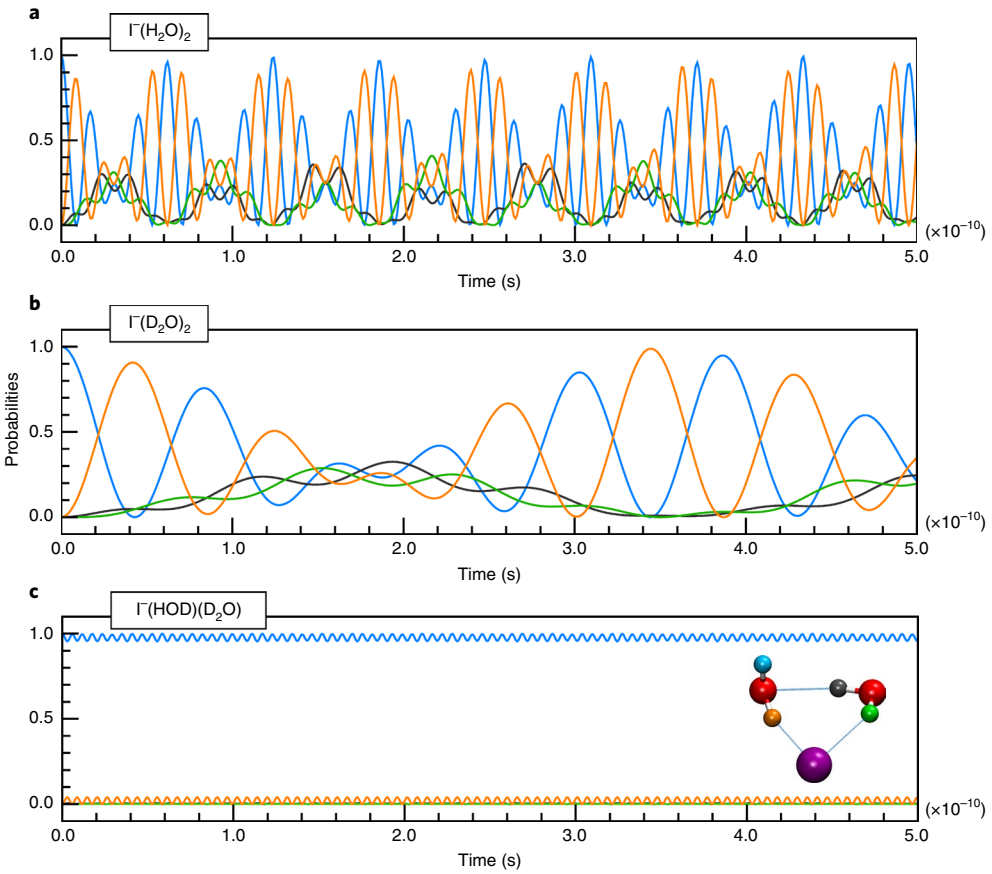

Fig. 3 | Tunnelling timescales in the isotopologues of the iodide–dihydrate complex. a, Time evolution of the probabilities for each of the four OH positions in the $I^-(H_2O)_2$ isotopologue, shown, with colours corresponding to those in the inset of **c**, to be occupied by the H atom located in the free OH position at time $t = 0$. **b**, Same analysis as in (**a**) performed for the OD positions in the $I^-(D_2O)_2$ isotopologue. **c**, Same analysis as in (**a**) performed for the OH positions in the $I^-(HOD)(D_2O)$ isotopologue. The $I^-(H_2O)_2$ isotopologue displays faster interchange between the four different positions than the analogous $I^-(D_2O)_2$ isotopologue due to the H atoms being lighter and, consequently, exhibiting more pronounced quantum-mechanical behaviour than the corresponding D atoms. The tunnelling dynamics are suppressed in the $I^-(HOD)(D_2O)$ isotopologue due to the asymmetric nature of the four hydrogen-bond arrangements. See main text for details.

equivalent positions through the same large amplitude rotational tunnelling motions identified by the RPI calculations. This complete 'scrambling' of hydrogen bonds emphasizes the purely quantum nature of both complexes at low temperature.

The interplay among ion–water and water–water interactions, entropic contributions and nuclear quantum effects in the iodide–dihydrate complex can be further characterized by investigating temperature-dependent hydrogen-bond rearrangements in the mixed isotopologue, $I^-(HOD)(D_2O)$. Isotopic substitution has been shown to be a powerful tool for determining hydrogen-bond rearrangements in water through vibrational spectroscopy, often enabling unambiguous spectral assignments that would otherwise be difficult to make due to strong intermode couplings[20]. Because the four distinct positions that the hydrogen atom can occupy within $I^-(HOD)(D_2O)$ are associated with different zero-point energies and entropic contributions, the total free energy of the complex in its closed configuration thus depends on the specific location of the hydrogen atom. As shown in Fig. 3c, the RPI calculations indicate that tunnelling in $I^-(HOD)(D_2O)$ is completely suppressed at low temperatures, with the hydrogen atom remaining locked-in in the free position. To monitor the evolution of the hydrogen-bond dynamics as a function of temperature, PIMD simulations were carried out to calculate the 2D quantum free energy surfaces (using the well-tempered metadynamics biasing approach[31]) along the H–O–I angle and H–O–I–O′ dihedral angle, which are employed as collective variables describing the iodide–water and water–water hydrogen-bond bifurcation motions, respectively (Fig. 5a,b). Also shown in Fig. 5d,e are the 1D quantum free energy curves associated with the two hydrogen-bond bifurcations along with the corresponding Born–Oppenheimer minimum potential energy paths, analogous to those shown in Fig. 4.

At 10 K, the configuration with the hydrogen atom in the free position still corresponds to the most stable structure of $I^-(HOD)(D_2O)$, lying approximately 0.1 kcal mol^{-1} below the other three configurations with the hydrogen atom in hydrogen-bonded positions. It should be noted that configuration 4 (Fig. 5c), with the hydrogen atom belonging to the DD water molecule and hydrogen-bonded to the iodide ion, is not part of any direct bifurcation pathway and can only be reached through a second-order dynamical process involving the iodide–water hydrogen-bond bifurcation followed by the water–water hydrogen-bond bifurcation pathways. Besides breaking the symmetry of the 1D quantum free energy profiles along both bifurcation pathways, the presence of the hydrogen atom in $I^-(HOD)(D_2O)$ also modifies the associated quantum free energy barriers, which become approximately three times higher than in the pure $I^-(H_2O)_2$ and $I^-(D_2O)_2$ complexes, but still appreciably lower than the corresponding barriers on the underlying Born–Oppenheimer potential energy surface. This suggests that tunnelling may possibly occur in $I^-(HOD)(D_2O)$ at finite temperature although to a lesser extent than in $I^-(H_2O)_2$ and $I^-(D_2O)_2$.

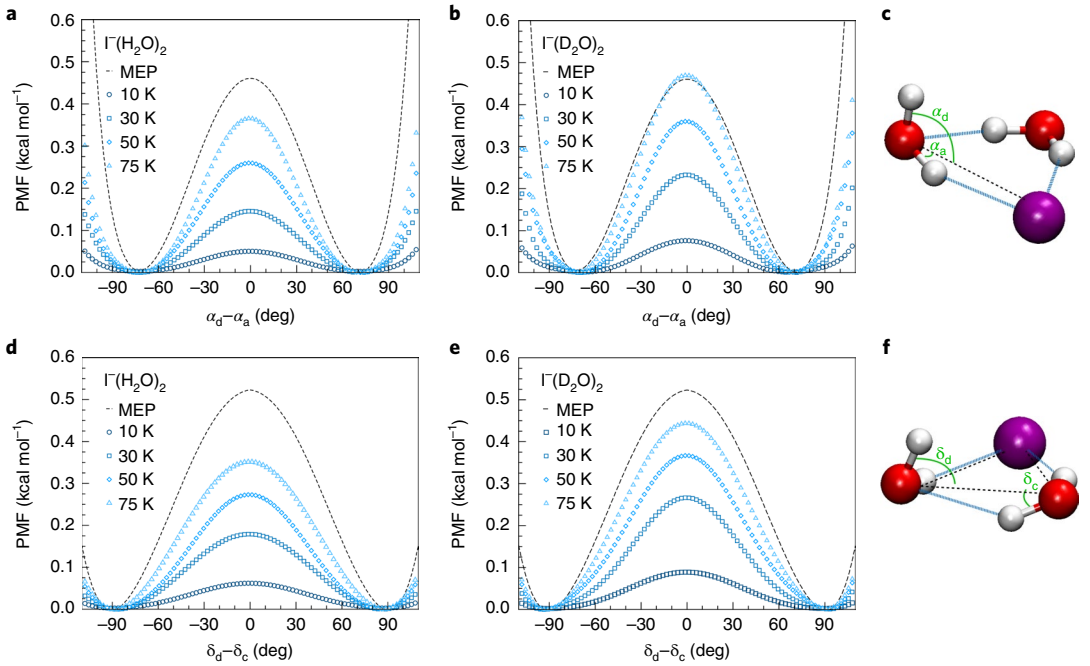

Fig. 4 | Temperature-dependent free energies along the tunnelling pathways. a,**b**, 1D quantum potential of mean forces (PMFs) along the iodide–water hydrogen-bond bifurcation pathway (defined by the collective variable $\alpha_d-\alpha_a$, where α_a and α_d are the two angles shown in the schematic in **c** of the $I^-(H_2O)_2$ and $I^-(D_2O)_2$ isotopologues, respectively, calculated from the corresponding PIMD simulations. **c**, Schematic representation of angles α_a and α_d in the iodide–dihydrate complex. **d**,**e**, 1D quantum PMFs along the water–water hydrogen-bond bifurcation pathway (defined by the collective variable $\delta_d-\delta_c$, where δ_c and δ_d are the two dihedrals shown in the schematic of **f** of the $I^-(H_2O)_2$ and $I^-(D_2O)_2$ isotopologues, respectively, calculated from the corresponding PIMD simulations. **f**, Schematic representation of dihedrals δ_c and δ_d in the iodide–dihydrate complex. At low temperature, the quantum free energies are significantly lower than the associated Born–Oppenheimer MEPs, demonstrating the highly quantum-mechanical nature of the iodide–dihydrate complex. As the temperature increases, the quantum free energies approach the MEP values, approaching transition to classical-like behaviour. See main text for details.

The average relative populations of the four different positions, however, will depend on the availability of accessible vibrational states at a particular temperature, governed by the Boltzmann distribution function. As shown in Fig. 5, configuration 2 is at least 0.1 kcal mol^{-1} lower in free energy than the other configurations, which corresponds to a temperature of ~50 K. Consequently, the other configurations will be stable and appreciably populated only at temperatures above 50 K.

Estimates of kinetic rates based on path-integral quantum transition state theory (PI-TST), neglecting any dynamical correction accounting for the possibility of barrier recrossing and quantum coherence, indicate that the timescales for both iodide–water and water–water hydrogen-bond bifurcations in $I^-(HOD)(D_2O)$ at 10 K are on the order of milliseconds, and between three and four orders of magnitude slower than in $I^-(H_2O)_2$ and $I^-(D_2O)_2$ (Supplementary Section 3). It should be noted, however, that PI-TST provides an approximation to a quantum rate, especially in the deep tunnelling regime at low temperature where, neglecting coherent dynamical effects, it can only be used to determine an upper bound for the actual quantum rate. In addition, compared to experiments, even small differences in barrier heights, which may be due to inaccuracies in the representation of the underlying Born–Oppenheimer potential energy surface, can result in large variations in the corresponding quantum rates. This implies that, in the present analysis, PI-TST rates can only serve to emphasize qualitative differences in the timescales associated with hydrogen-bond rearrangements in $I^-(H_2O)_2$ and $I^-(D_2O)_2$, on the one side, and $I^-(HOD)(D_2O)$, on the other. As the temperature increases, both 1D quantum free energy profiles associated with the iodide–water and water–water hydrogen-bond bifurcations approach the corresponding Born–Oppenheimer MEPs, leading to significantly faster hydrogen-bond rearrangements. At 50 K, PI-TST predicts timescales on the order of tens of nanoseconds for both bifurcations in $I^-(HOD)(D_2O)$, similar to those predicted for $I^-(H_2O)_2$ and $I^-(D_2O)_2$. Importantly, compared to 10 K, the 2D free energy surfaces shown in Fig. 5 indicates that both hydrogen-bonded positions of the DD water molecule become relatively more stable at 50 K. This implies that local differences in zero-point energies become increasingly less important as the temperature increases, which thus explains the similarity of the PI-TST rates predicted for the three different isotopologues at 50 K.

Discussion

By combining accurate many-body representations of iodide–water and water–water interactions with state-of-the-art quantum dynamics simulations, this study provides first evidence for the existence of tunnelling pathways in $I^-(H_2O)_2$. A detailed analysis of the underlying mechanisms indicates that tunnelling leads to fast hydrogen-bond rearrangements mediated by the iodide ion. These rearrangements involve large-amplitude rotations of the water OH bonds and result in the four hydrogen atoms exchanging their positions on a picosecond timescale even at low temperature. Identical pathways are observed, following isotopic substitution, in $I^-(D_2O)_2$, although the associated hydrogen-bond dynamics is significantly slowed down. Further insights into the competition between iodide–water and water–water interactions as well as the role played by nuclear quantum effects are gained from analysis of the hydrogen-bond rearrangements in the $I^-(HOD)(D_2O)$ isotopologue. By breaking the symmetry along the tunnelling pathways, the presence of the hydrogen atom allows for precisely probing quantum free energies

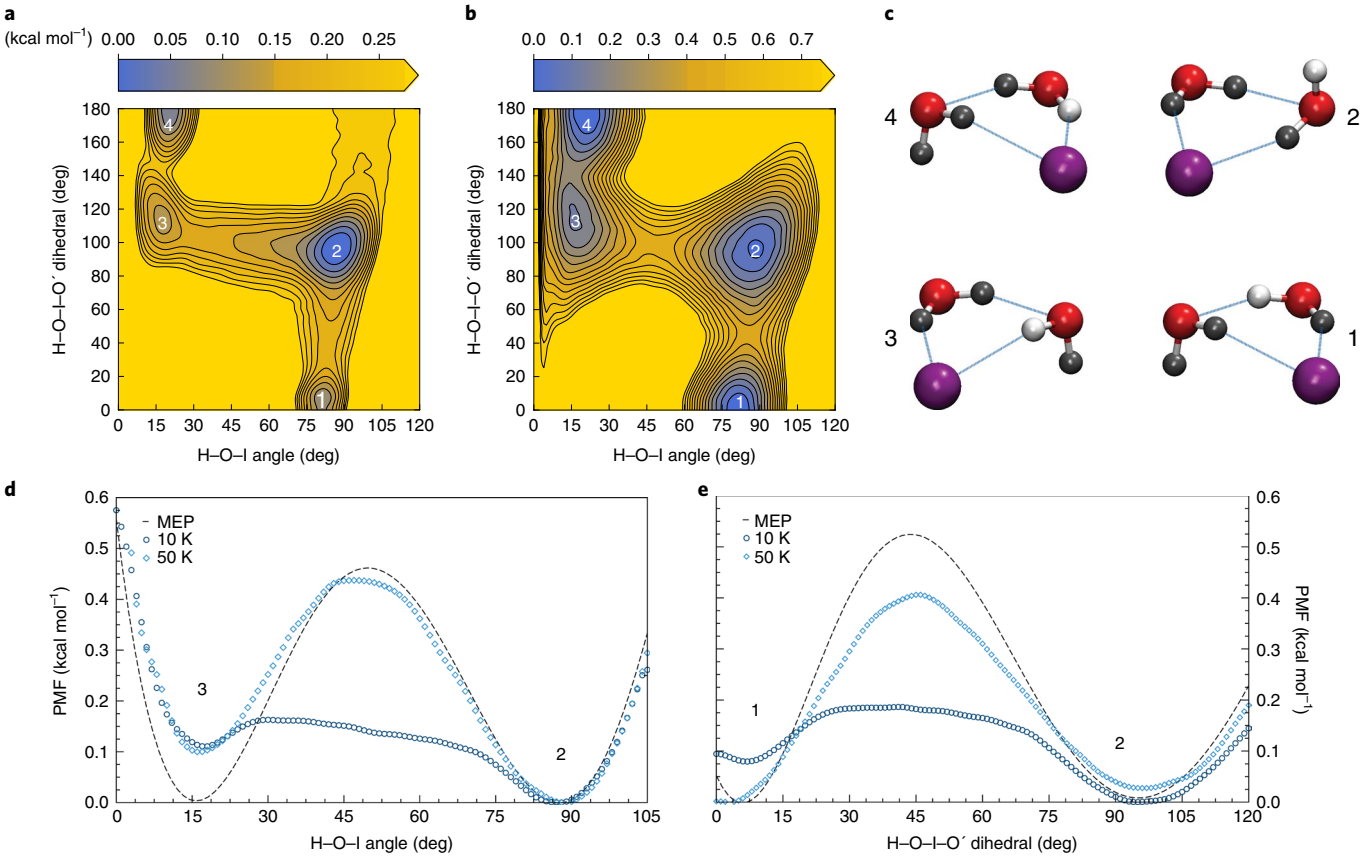

Fig. 5 | Determining local free energies associated with different hydrogen-bonding environments in the $I^-(HOD)(D_2O)$ isotopologue of the iodide–dihydrate complex. a,**b**, 2D quantum PMFs along the iodide–water and water–water hydrogen-bond bifurcation pathways (defined by the H–O–I angle on the *x* axis and the H–O–I–O′ dihedral on the *y* axis, respectively) of the $I^-(HOD)(D_2O)$ isotopologue calculated from PIMD well-tempered metadynamics simulations carried out at 10 K (**a**) and 50 K (**b**). Also indicated with 1, 2, 3 and 4 are the hydrogen-bond arrangements corresponding to the schematic representations shown in **c**. **c**, Schematic representations of the four hydrogen-bonding environments experienced by the H atom in the $I^-(HOD)(D_2O)$ isotopologue. The O, H and D atoms are shown in red, white and grey, respectively. **d**,**e**, 1D quantum PMFs along the H–O–I angle and H–O–I–O′ dihedral of the $I^-(HOD)(D_2O)$ isotopologue, respectively, calculated from PIMD well-tempered metadynamics simulations. Also indicated with 1, 2 and 3 are the hydrogen-bond arrangements corresponding to the schematic representations shown in **c**.

associated with the four different bonding topologies within the complex. Due to local differences in the zero-point energies and entropic contributions, it is found that interconversion between the four different isotopomers of $I^-(HOD)(D_2O)$ is largely suppressed at low temperature, indicating that the mechanisms associated with hydrogen-bond rearrangements in the iodide–dihydrate complex can effectively be manipulated by isotopic substitutions. As the temperature increases, nuclear quantum effects become progressively less important, with all different isotopologues exhibiting similar hydrogen-bond dynamics above 75 K. It is interesting to note that, alternatively to an increase in temperature, the interconversion in $I^-(HOD)(D_2O)$ could be facilitated by an inert 'messenger-tag' molecule like D_2 or Ar (commonly used in predissociation vibrational spectroscopy), which would increase the density of states that are accessible at low temperatures.

Compared to the water trimer, the present results demonstrate that the iodide ion weakens the water–water hydrogen bond, leading to significantly faster tunnelling dynamics. Importantly, the flip rotation, which is the fastest motion in the water trimer, becomes the slowest in the iodide–dihydrate complex due to a higher rotational barrier resulting from iodide–water interactions. Although these results clearly indicate that the iodide ion perturbs water–water hydrogen-bond rearrangements, the predicted faster dynamics in the iodide–dihydrate complex is apparently at odds with the ultrafast vibrational spectroscopy measurements of salt solutions, suggesting that the hydrogen-bond dynamics within the first hydration shell of iodide is significantly slowed compared to that of pure water. This difference can be attributed to the presence of a free OH bond in the iodide–dihydrate complex, which effectively triggers the overall hydrogen-bond rearrangement within the complex and enable faster water reorientation along both iodide–water and water–water hydrogen-bond bifurcation pathways. In turn, the present quantum simulations of the iodide–dihydrate complex provide indirect evidence for the importance of cooperative effects in water hydrogen-bond rearrangements around iodide ions in solution, which, involving water molecules beyond the first hydration shell, thus slows down the overall dynamics, reversing the trend observed in the gas phase.

The present theoretical analysis thus raises the possibility that faster hydrogen-bond dynamics in the first hydration shell of iodide ions may be observed in frustrated systems, such as interfaces, where water molecules hydrogen-bonded to the ion can be undercoordinated, with at least one dangling OH bond. Furthermore, because the hydrogen-bond rearrangement pathways identified in the iodide–dihydrate complex directly depend on the nature of the iodide–water interaction, ion-specific effects on the hydrogen-bond dynamics are predicted to also exist in chloride–dihydrate and bromide–dihydrate complexes, which display similar minimum-energy cyclic structures, and possibly in the first hydration shell of both chloride and bromide ions in solution. Ion-dependent

hydrogen-bond rearrangements through tunnelling may thus exist at the surface of salt solutions where, mediating surface-specific ion effects[6], they can have direct implications for heterogeneous interfacial chemical processes[32].

Methods

In all calculations the iodide–water interactions are described by the corresponding many-body MB-nrg PEF introduced in refs. [18,24]. PIMD simulations[33] were performed to investigate the temperature dependence of the equilibrium between 'closed' and 'open' configurations of the iodide–dihydrate complex. In these PIMD simulations, each atom is represented by a Feynman ring polymer[34] with a variable number of beads depending on the temperature. RPI calculations[35,36] were performed to identify the tunnelling pathways and corresponding tunnelling splitting patterns for the $I^-(H_2O)_2$ and $I^-(D_2O)_2$ complexes. Quantum free energies for the two hydrogen-bond bifurcation pathways in the $I^-(HOD)(D_2O)$ complex were calculated from biased PIMD simulations carried out at 10 K and 50 K using the well-tempered metadynamics method[31,37] as implemented in the PLUMED plugin[38]. For these simulations, the H–O–I angle and H–O–I–O′ dihedral in the $I^-(HOD)(D_2O)$ complex, which are calculated from the centroid of the ring polymers associated with the relevant atoms in the PIMD simulations, were chosen as the collective variables to map the underlying quantum free energies. Specific details for the PIMD, RPI and well-tempered metadynamics simulations are reported in Supplementary Section 1.

Code availability

The computer codes used in this study are available from the authors upon request.

Data availability

Any data generated and analysed for this study that are not included in this Article and its Supplementary Information are available from the authors upon request.

Received: 21 June 2018; Accepted: 22 January 2019;
Published online: 4 March 2019

References

1. Sneen, R. A. Substitution at a saturated carbon atom. XVII. Organic ion pairs as intermediates in nucleophilic substitution and elimination reactions. *Acc. Chem. Res.* **6**, 46–53 (1973).
2. Pregel, M., Dunn, E., Nagelkerke, R., Thatcher, G. & Buncel, E. Alkali–metal ion catalysis and inhibition in nucleophilic displacement reaction of phosphorus–sulfur–and carbon–based esters. *Chem. Soc. Rev.* **24**, 449–455 (1995).
3. Collins, K. D., Neilson, G. W. & Enderby, J. E. Ions in water: characterizing the forces that control chemical processes and biological structure. *Biophys. Chem.* **128**, 95–104 (2007).
4. Kunz, W. Specific ion effects in colloidal and biological systems. *Curr. Opin. Colloid Interface Sci.* **15**, 34–39 (2010).
5. Nostro, P. L. & Ninham, B. W. Hofmeister phenomena: an update on ion specificity in biology. *Chem. Rev.* **112**, 2287–2322 (2012).
6. Tobias, D. J., Stern, A. C., Baer, M. D., Levin, Y. & Mundy, C. J. Simulation and theory of ions at atmospherically relevant aqueous liquid–air interfaces. *Annu. Rev. Phys. Chem.* **64**, 339–359 (2013).
7. Lehtipalo, K. et al. The effect of acid–base clustering and ions on the growth of atmospheric nano-particles. *Nat. Commun.* **7**, 11594 (2016).
8. Winter, M. & Brodd, R. J. What are batteries, fuel cells, and supercapacitors? *Chem. Rev.* **104**, 4245–4270 (2004).
9. Pollard, T. P. & Beck, T. L. Toward a quantitative theory of hofmeister phenomena: from quantum effects to thermodynamics. *Curr. Opin. Colloid Interface Sci.* **23**, 110–118 (2016).
10. Bakker, H., Kropman, M. & Omta, A. Effect of ions on the structure and dynamics of liquid water. *J. Phys. Condens. Matter* **17**, S3215 (2005).
11. Jungwirth, P. & Tobias, D. J. Specific ion effects at the air/water interface. *Chem. Rev.* **106**, 1259–1281 (2006).
12. Robertson, W. H. & Johnson, M. A. Molecular aspects of halide ion hydration: the cluster approach. *Annu. Rev. Phys. Chem.* **54**, 173–213 (2003).
13. Ayala, R., Martinez, J. M., Pappalardo, R. R. & Marcos, E. S. Study of the stabilization energies of halide–water clusters: an application of first-principles interaction potentials based on a polarizable and flexible model. *J. Chem. Phys.* **121**, 7269–7275 (2004).
14. Kamarchik, E. & Bowman, J. M. Quantum vibrational analysis of hydrated ions using an ab initio potential. *J. Phys. Chem. A* **114**, 12945–12951 (2010).
15. Wang, X.-G. & Carrington, T. Jr. Rovibrational levels and wavefunctions of Cl^-H_2O. *J. Chem. Phys.* **140**, 204306 (2014).
16. Kamarchik, E., Toffoli, D., Christiansen, O. & Bowman, J. M. Ab initio potential energy and dipole moment surfaces of the $F^-(H_2O)$ complex. *Spectrochim. Acta A* **119**, 59–62 (2014).
17. Sarka, J., Lauvergnat, D., Brites, V., Császár, A. G. & Léonard, C. Rovibrational energy levels of the $F^-(H_2O)$ and $F^-(D_2O)$ complexes. *Phys. Chem. Chem. Phys.* **18**, 17678–17690 (2016).
18. Bajaj, P., Wang, X.-G., Carrington, T. Jr. & Paesani, F. Vibrational spectra of halide–water dimers: insights on ion hydration from full-dimensional quantum calculations on many-body potential energy surfaces. *J. Chem. Phys.* **148**, 102321 (2018).
19. Wolke, C. T. et al. Thermodynamics of water dimer dissociation in the primary hydration shell of the iodide ion with temperature-dependent vibrational predissociation spectroscopy. *J. Phys. Chem. A* **119**, 1859–1866 (2015).
20. Yang, N., Duong, C. H., Kelleher, P. J., Johnson, M. A. & McCoy, A. B. Isolation of site-specific anharmonicities of individual water molecules in the $I^-(H_2O)_2$ complex using tag-free, isotopomer selective IR-IR double resonance. *Chem. Phys. Lett.* **690**, 159–171 (2017).
21. Cheng, X. & Steele, R. P. Efficient anharmonic vibrational spectroscopy for large molecules using local-mode coordinates. *J. Chem. Phys.* **141**, 104105 (2014).
22. Cheng, X., Talbot, J. J. & Steele, R. P. Tuning vibrational mode localization with frequency windowing. *J. Chem. Phys.* **145**, 124112 (2016).
23. Wang, Y. & Bowman, J. M. Ab initio potential and dipole moment surfaces for water. II. Local-monomer calculations of the infrared spectra of water clusters. *J. Chem. Phys.* **134**, 154510 (2011).
24. Bajaj, P., Götz, A. W. & Paesani, F. Toward chemical accuracy in description of ion–water interactions through many-body representations. I. Halide–water dimer potential energy surfaces. *J. Chem. Theory Comput.* **12**, 2698–2705 (2016).
25. Brown, S. E. et al. Monitoring water clusters 'melt' through vibrational spectroscopy. *J. Am. Chem. Soc.* **139**, 7082–7088 (2017).
26. Pugliano, N. & Saykally, R. J. Measurement of quantum tunneling between chiral isomers of the cyclic water trimer. *Science* **257**, 1937–1940 (1992).
27. Keutsch, F. N. & Saykally, R. J. Water clusters: untangling the mysteries of the liquid, one molecule at a time. *Proc. Natl Acad. Sci. USA* **98**, 10533–10540 (2001).
28. Keutsch, F. N., Cruzan, J. D. & Saykally, R. J. The water trimer. *Chem. Rev.* **103**, 2533–2578 (2003).
29. Richardson, J. O., Althorpe, S. C. & Wales, D. J. Instanton calculations of tunneling splittings for water dimer and trimer. *J. Chem. Phys.* **135**, 124109 (2011).
30. Richardson, J. O. & Althorpe, S. C. Ring-polymer instanton method for calculating tunneling splittings. *J. Chem. Phys.* **134**, 054109 (2011).
31. Barducci, A., Bussi, G. & Parrinello, M. Well-tempered metadynamics: a smoothly converging and tunable free-energy method. *Phys. Rev. Lett.* **100**, 020603 (2008).
32. Knipping, E. M. et al. Experiments and simulations of ion-enhanced interfacial chemistry on aqueous NaCl aerosols. *Science* **288**, 301–306 (2000).
33. Parrinello, M. & Rahman, A. Study of an F center in molten KCl. *J. Chem. Phys.* **80**, 860–867 (1984).
34. Feynman, R. P. *Statistical Mechanics: A Set of Lectures* (Benjamin, New York, 1972).
35. Richardson, J. O. Perspective: ring-polymer instanton theory. *J. Chem. Phys.* **148**, 200901 (2018).
36. Richardson, J. O. Ring-polymer instanton theory. *Int. Rev. Phys. Chem.* **37**, 171–216 (2018).
37. Laio, A. & Parrinello, M. Escaping free-energy minima. *Proc. Natl Acad. Sci. USA* **99**, 12562–12566 (2002).
38. Tribello, G. A., Bonomi, M., Branduardi, D., Camilloni, C. & Bussi, G. PLUMED 2: new feathers for an old bird. *Comput. Phys. Commun.* **185**, 604–613 (2014).

Acknowledgements

The authors thank M.A. Johnson and N. Yang for stimulating discussions about the vibrational spectroscopy and dynamics of the $I^-(H_2O)_2$ complex and its isotopologues. This research was supported by the National Science Foundation Center for Chemical Innovation 'Center for Aerosol Impacts on Chemistry of the Environment' (grant no. CHE-1305427) and by the Swiss National Science Foundation (project no. 175696). Calculations were performed using the Extreme Science and Engineering Discovery Environment (XSEDE), which is supported by the National Science Foundation (grant no. ACI-1053575, allocation TG-CHE110009), the High Performance Computing Modernization Program (HPCMP), which is supported by the Air Force Office of Scientific Research (grant no. FA9550-16-1-0327), as well as the Triton Shared Computing Cluster (TSCC) at the San Diego Supercomputer Center.

Author contributions

P.B. performed all simulations, contributed to data analysis and co-wrote the paper. J.O.R. guided the RPI calculations, contributed to data analysis and co-wrote the paper. F.P. initiated the project, guided the simulation design and data analysis, and co-wrote the paper.

Competing interests

The authors declare no competing interests.

Additional information

Supplementary information is available for this paper at https://doi.org/10.1038/s41557-019-0220-2.

Correspondence and requests for materials should be addressed to F.P.